Modulation of millimetre-wave and THz properties of IMPATT sources via external magnetic field

Partha Banerjee

Department of Electronics and Communication Engineering,
Academy of Technology,
Adisaptagram, Hooghly,
WB – 712121, India
Email: parthabanerjee21@gmail.com

Aritra Acharyya*

Department of Electronics and Communication Engineering,
Cooch Behar Government Engineering College,
Harinchawra, Ghughumari,
WB – 736170, India
Email: ari_besu@yahoo.co.in
*Corresponding author

Arindam Biswas

Department of Mining Engineering,
Kazi Nazrul University,
Asansol, Burdwan,
WB – 713340, India
Email: mailarindambiswas@yahoo.co.in

A.K. Bhattacharjee

Department of Electronics and Communication Engineering,
National Institute of Technology,
Dugrapur, WB – 713209, India
Email: akbece12@yahoo.com

Abstract: The modulation of millimetre-wave (mm-wave) and terahertz (THz) properties of impact avalanche transit time (IMPATT) sources under external steady magnetic field has been studied in this paper. The arrangement of magnetic field tuning of IMPATT oscillators by using external transverse steady magnetic field is referred to as magnetic field tunable avalanche transit time (MAGTATT) oscillators. The sensitivities of various static, large-signal and noise characteristics of silicon-based MAGTATT sources operating at mm-wave atmospheric window frequencies (94, 140 and 220 GHz) and two different THz frequencies (0.3 and 0.5 THz) have been studied. Comprehensive two-dimensional simulation models developed by the authors for evaluating static, large-signal and noise characteristics of MATATT diodes have been

used for this purpose. The simulation results show that the above-mentioned magnetic field sensitivities of the device properties are significantly reduced with the increase of the operating frequency.

Keywords: atmospheric window frequency; MAGTATT; sensitivity analysis; terahertz; THz.

Reference to this paper should be made as follows: Banerjee, P., Acharyya, A., Biswas, A. and Bhattacharjee, A.K. (2020) 'Modulation of millimetre-wave and THz properties of IMPATT sources via external magnetic field', *Int. J. Nanoparticles*, Vol. 12, Nos. 1/2, pp.17–32.

Biographical notes: Partha Banerjee is presently carrying out his Doctoral Research at National Institute of Technology, Dugapur, WB, India. His research interests are high frequency semiconductor devices.

Aritra Acharyya received his BE and MTech from the IIEST, Shibpur, India, and Institute of Radio Physics and Electronics, University of Calcutta, India, in 2007 and 2010 respectively. Finally he obtained his PhD from the Institute of Radio Physics and Electronics, University of Calcutta, in 2016. His research interests are high frequency semiconductor devices. He has already published more than 135 research papers in peer reviewed journals and conference proceedings.

Arindam Biswas received his BTech and MTech from the Dumkal Institute of Engineering and Technology, WB, India, and Institute of Radio Physics and Electronics, University of Calcutta, in 2007 and 2010 respectively. Finally he obtained his PhD from the National Institute of Technology, Dugapur, WB, India, in 2013. His research interests are nonlinear optics and high frequency semiconductor devices.

A.K. Bhattacharjee is currently working as a Professor of ECE Department in the National Institute of Technology, Dugapur, WB, India. His research interests are antenna and high frequency semiconductor devices.

This paper is a revised and expanded version of a paper entitled 'Millimeter-wave and terahertz magnetic field tunable avalanche transit time sources' presented at IEEE EDKCON 2018.

1 Introduction

The terahertz (THz) frequency spectrum (0.3–10.0 THz) offers several fascinating applications such as ultrahigh-speed wireless communication, biomedical screening, remote sensing of explosive materials, food diagnostic, inspection of interstellar medium and planetary atmosphere, short range terrestrial and airborne communication, space-base communication, spectroscopy, quality inspection in various industrial branches, etc. (Martyniuk et al., 2014; Siegel, 2007; Grischkowsky et al., 1990; Debus and Bolivar, 2007; Yasui et al., 2005; Stoik et al., 2008; Jördens and Koch, 2008; Fitzgerald et al., 2005; Ward et al., 2004; Heyminck et al., 2009; Crowe et al., 2011a, 2011b; Maestrini et al., 2012). Moreover, the THz waves are highly suitable for bio-sensing, bio-imaging, and various medical and pharmaceutical applications (Siegel, 2004). However, THz

frequency generation with sufficiently high power is a challenging field of research. Still now, the terahertz-gap (0.3–10.0 THz) is considered as an unexploited frequency spectrum due to the unavailability of commercial THz source (Tonouchi, 2007). Some solid-state sources like quantum cascade lasers (QCLs), resonant tunnelling diodes (RTDs), high electron mobility transistor (HEMTs), heterojunction bipolar transistors (HBTs), etc. are capable of generating THz waves at room temperature (Williams, 2007; Lai et al., 2007; Deal et al., 2010; Urteaga et al., 2010; Lobisser et al., 2009; Seo et al., 2010; Hacker et al., 2010; Seo et al., 2011; Kitagawa et al., 2017). However, those are limited in output power; only a few micro-watts (μW) of THz power can be delivered by those. Since last decade, several researchers have explored the potentialities of wide bandgap material-base impact avalanche transit time (IMPATT) oscillators as THz frequency radiators (Acharyya and Banerjee, 2014; Acharyya et al., 2015; Biswas et al., 2018).

It is not sufficient to generate fixed frequency THz waves for the applications related to wireless communication. Therefore, the frequency tuning of THz oscillator is an important aspect to be studied in details. There are four different techniques available for frequency tuning of IMPATT oscillators, those are

1 mechanical tuning

2 electronic tuning

3 optical tuning

4 magnetic field tuning; out of these four techniques, first two are manual techniques and last two are automatic techniques.

Mechanical tuning technique cannot be used for direct modulation, since it is completely manual in nature and no message can be embedded into the generated wave via this technique; also the achievable tuning frequency range is very small by using this technique (Gibbons, 1973). Though the larger range of frequency tuning is achievable by using bias current of electronic tuning technique, it is also unable to serve the purpose of direct frequency modulation due to its manual nature (Gilden and Hines, 1966). Optical tuning mechanism utilises the photon-electron interaction inside the IMPATT diode; a light source of appropriate wavelength has to be illuminated on the active region of the device via a tiny hole created on any of the metal electrode (Schweighart et al., 1978; Vyas et al., 1979; Forrest and Seeds, 1978; Seeds and Augusto, 1990; Acharyya et al., 2014a, 2014b, 2014c). It is an efficient frequency tuning technique and also the direct modulation of message signal (illuminated from the optical source) into the THz wave is possible in this case. However, the creation of tiny hole on any of the electrodes (creating optical window) for photo injection into the device is a challenging task, especially at the dimensions [in the order of nano-metres (nm)] associated with THz IMPATTs. On the other hand, magnetic field tuning of the THz IMPATT sources utilises the deflection of moving charge carriers under electric field via externally applied static or time varying magnetic field along transverse direction (Glance, 1973; Pucel and Masse, 1972; Hartnagel et al., 1975; Baltes et al., 1984; Pfleiderer, 1972; Banerjee et al., 2016a, 2018, 2016b). This technique can serve the purpose of direct modulation of message signal into THz wave. The advantage of this technique that there is no need of any special structural modification in the IMPATT diode and oscillator circuitry; only the external magnetic field generator has to be placed across the IMPATT oscillator such that the direction of

the magnetic field remains transverse with respect to the direction of current flow through the IMPATT diode.

In early '70s, several researchers reported the potentiality of magnetic field tuning of IMPATT oscillators by experimentally demonstrating the power and frequency modulation of IMPATT sources by applying external magnetic field (Glance, 1973; Hartnagel et al., 1975). The experiments were primarily carried out on X-band (8–12 GHz) Si-base IMPATT oscillators (Glance, 1973; Hartnagel et al., 1975) and significant amount of frequency shift of the source due to the application of external transverse magnetic field were achieved at that frequency band. However, the phenomena of magnetic field tuning of IMPATT oscillators were not well understood at that time; the magnetic field induced change in carrier motion, re-distribution of charge carriers and electric potential were simply explained in terms of Hall voltage and corresponding carrier deflection (Baltes et al., 1984; Pfleiderer, 1972). The complete modelling of the above-mentioned phenomena was not developed by any researcher during that period and consequently they could have lost motivation to implement magnetic field modulated IMPATT sources at higher microwave or mm-wave frequency bands.

In 2016, Banerjee et al. (2016a, 2018, 2016b) reported complete two dimensional (2D) models for the analysis of static (DC), large-signal (L-S) and noise characteristics of IMPATT sources operating at W-band (75–110 GHz) under external transverse magnetic field. The proposed arrangement was referred to as magnetic field tunable avalanche transit time (MAGTATT) source. They reported the sensitivities of DC, L-S and noise properties of a 94 GHz MAGTATT source by means of the simulation results obtained from the 2D models developed by them.

In the present paper, the authors have further studied the above-mentioned magnetic field sensitivities of MAGTATT sources operating at higher frequency bands such as 140 GHz, 220 GHz, 0.3 THz and 0.5 THz.

2 Simulation method

The shape of the cross-section of DDR IMPATT diode is considered to be rectangular instead of circular. This consideration simplifies the 2D device modelling as well as the modelling of external magnetic field coupling arrangement. Here we can easily deploy convenient Cartesian coordinate system instead of more complicated cylindrical coordinate system. Choice of the shape of the cross-section of the diodes do not influence the simulation results since here only the cross-sectional area is important (shape of the cross-section is unimportant). If a diode having circular cross-section possesses junction diameter D_j, the corresponding cross-sectional junction area is $A_j = \pi D_j^2 / 4$; the same cross-sectional area of a rectangular cross-section diode is given by $A_j = DH$, where D is the width (along x-direction) and H is the height (along z-direction). Therefore, by equating the above-mentioned circular and rectangular cross-sectional areas, we obtain $H = \pi D_j^2 / 4D$; by choosing the suitable value of the width D, one can obtain the height H of the diode for a given value of circular cross-section junction diameter D_j. The 3D model of the device is shown in Figure 1. The carrier transport across the diode is considered to be occurred along $\pm y$-direction (transport of electrons and holes along $+y$-direction and $-y$-direction respectively) in absence of external magnetic field. The

presence of external steady magnetic field along z-direction ($\vec{B} \equiv (0, 0, B_z)$), the Lorentz force deflects charge carriers along the Hall direction, i.e., along $\pm x$-direction depending on the polarity of charge carriers and direction of applied magnetic field ($\pm z$-direction) (Banerjee et al., 2016a).

Figure 1 3D model rectangular cross-section of DDR IMPATT diode used in simulation

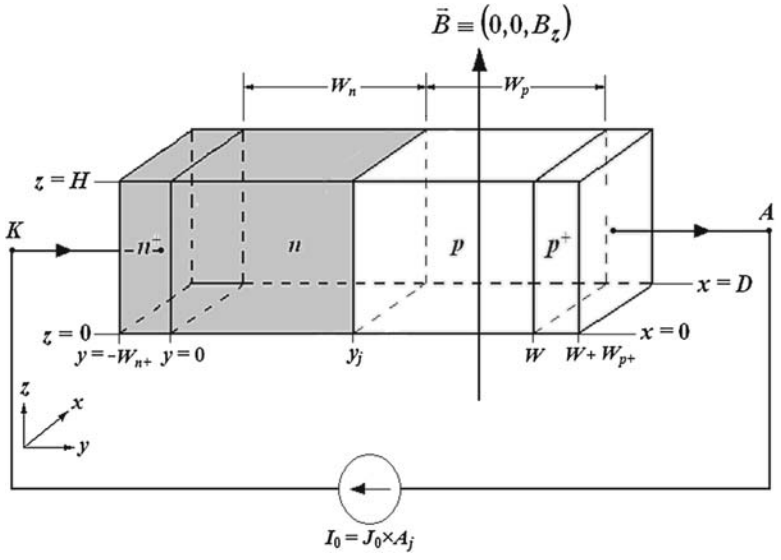

Since the deflection of charge carriers flowing along $\pm y$-direction across the diode are bound to occur along $\pm x$-direction as mentioned earlier. The distributions of charge carriers within the device are only functions of space coordinates x and y, and obviously independent of z-coordinate. Thus, the model under consideration is reduced to 2D problem having only x and y coordinates.

The 2D models of static (DC), L-S and noise of free running reverse biased DDR IMPATT oscillators have already been reported by the authors earlier (Banerjee et al., 2016a, 2018, 2016b). In this work, the simulations have been carried out by adopting the same simulation methodologies (Banerjee et al., 2016a, 2018, 2016b).

The flowchart of the entire simulation task is given in Figure 2. The simulation methodology has been described is following points:

1 At first a diode based on Si, designed to operate at a particular frequency (f_d) has been selected for simulation.

2 Design frequency (f_d) and design parameters (structural and doping parameters) have been given as the inputs of the simulation program.

3 The magnitude of the range of applied external transverse magnetic field strength ($|B_z| = 0 – 5$ Tesla) has been given as another input of the simulation program.

4 Bias current density (J_0) value is also given as the final input of the simulation program.

5 Next, the 2D DC characteristics of the diode are obtained for a given J_0 value and pre-selected range of $|B_z|$ as the outcomes of 2D static simulation program (Yasui et al., 2005). Output DC parameters are stored in memory.

6 Next, the 2D L-S program is run and L-S parameters of the diode for a given J_0 value and pre-selected range of $|B_z|$ are obtained (Banerjee et al., 2016a); those are also stored in memory.

7 Next, the 2D noise program is run and noise parameters of the diode for a given J_0 value and pre-selected range of $|B_z|$ are obtained (Banerjee et al., 2018, 2016b); those are also stored in memory.

8 Finally, the sensitivity analysis of DC, L-S and noise parameters already stored in memory are carried out.

The sensitivity of DC, L-S and noise parameters with respect to applied external magnetic field is defined as (Banerjee et al., 2016a)

$$S_X = \left|\frac{\Delta X}{\Delta B_z}\right| B_z = B_f \tag{1}$$

where X is the static or L-S or noise parameter under consideration, $\Delta X = X_f - X_i$ and $\Delta B_z = B_f - B_i$; where X_f and B_f are the values of the parameter and magnetic field respectively for which the sensitivity is to be calculated and X_i and B_i are the values of the parameter and magnetic field respectively just smaller than X_f and B_f.

3 Design of the device structure

The structural and doping parameters of the diodes operating at 94, 140, 220, 300 and 500 GHz frequencies as well as corresponding bias current densities have been designed and optimised subject to obtain maximum DC to RF conversion efficiency of the sources. The details of the design procedure have already been reported earlier by the authors (Acharyya et al., 2013a). The dimensions of n- and p-epitaxial layers (W_n and W_p), corresponding doping densities (N_D and N_A) and associated optimum bias current densities (J_0) of 94, 140, 220, 300 and 500 GHz diodes have been pictorially illustrated by Figure 3 via a 3D plot. The aforementioned diodes are referred as MT1, MT2, MT3, MT4 and MT5 respectively. The doping concentrations of n^+- and p^+-contact layers have been chosen to be ~1,025 m^{-3}. The junction diameter (D_j) of the circular cross-section diodes are given by 35, 25, 20, 15 and 10 μm and corresponding junction areas (A_j) are given by 9.6210×10^{-10}, 9.6210×10^{-10}, 4.9090×10^{-10}, 3.1420×10^{-10} and 0.785×10^{-10} respectively. If the width (D) of all the rectangular cross-section diodes are chosen as D = 10 μm, then the height (H) of those are given by 96.21, 49.09, 31.42, 17.67 and 7.85 μm respectively.

4 Material parameters

The electric field dependent ionisation rates of (α_n, α_p), drift velocities (v_n, v_p) of charge carriers, other material parameters like energy bandgap (E_g), density of state effective

mass (m_d*), permittivity (ε_r), effective density of state of conduction and valence bands (N_c, N_v), mobilities (μ_n, μ_p), diffusivity (D_n, D_p), diffusion length (L_n, L_p) of electron and holes in Si measured at 500 K are taken from published literature for simulation (Grant, 1973; Canali et al., 1971; IOFFE, 2019; Zeghbroeck, 2011). Table 1 lists the material parameters of Si at 500 K.

Table 1 Important material parameters of Si at 500 K

Electric field dependent material parameter	*Electric field range, ξ ($\times 10^7$ V m^{-1})*	*Value*	*Other material parameter*	*Value*
* A_n ($\times 10^9$ m^{-1}) (Grant, 1973)	2.40–5.30	0.0620	E_g (eV) (IOFFE, 2019; Zeghbroeck, 2011)	1.0465
* A_n ($\times 10^9$ m^{-1}) (Grant, 1973)	5.30–7.70	0.0500	¶ m_d* ($\times m_0$) (IOFFE, 2019)	0.1370
* B_n ($\times 10^9$ V m^{-1}) (Grant, 1973)	2.40–5.30	0.1340	¶¶ ε_r (IOFFE, 2019)	11.7000
* B_n ($\times 10^9$ V m^{-1}) (Grant, 1973)	5.30–7.70	0.1250	n_i ($\times$1,013 m^{-3}) (IOFFE, 2019)	859.5800
* A_p ($\times 10^9$ m^{-1}) (Grant, 1973)	2.40–5.30	0.2000	N_c ($\times$1,025 m^{-3}) (IOFFE, 2019)	6.9318
* A_p ($\times 10^9$ m^{-1}) (Grant, 1973)	5.30–7.70	0.0560	N_v ($\times$1,025 m^{-3}) (IOFFE, 2019)	3.9131
* B_p ($\times 10^9$ V m^{-1}) (Grant, 1973)	2.40–5.30	0.2190	μ_n (m^2 V^{-1} s^{-1}) (IOFFE, 2019)	0.0500
* B_p ($\times 10^9$ V m^{-1}) (Grant, 1973)	5.30–7.70	0.1540	μ_p (m^2 V^{-1} s^{-1}) (IOFFE, 2019)	0.0180
* m_α (Grant, 1973)	2.40–7.70	1.0000	D_n ($\times 10^{-4}$ m^2 s^{-1}) (IOFFE, 2019; Zeghbroeck, 2011)	11.0000
** v_{sn} ($\times 10^5$ m s^{-1}) (Canali et al., 1971)	2.40–7.70	0.6430	D_p ($\times 10^{-4}$ m^2 s^{-1}) (IOFFE, 2019; Zeghbroeck, 2011)	1.8900
** v_{sp} ($\times 10^5$ m s^{-1}) (Canali et al., 1971)	2.40–7.70	0.6340	L_n ($\times 10^{-6}$ m) (IOFFE, 2019; Zeghbroeck, 2011)	35.4000
---	---	---	L_p ($\times 10^{-6}$ m) (IOFFE, 2019; Zeghbroeck, 2011)	10.0000

Notes: *ionisation rate of electrons and holes $\alpha_{n,p}(\xi) = A_{n,p}\exp[(-B_{n,p}/\xi)^{m_\alpha}]$ as functions of electric field (ξ) (Grant, 1973).
**drift velocity of electrons and holes $v_{n,p}(\xi) = v_{sn,sp}[1-\exp(-\mu_{n,p}\xi / v_{sn,sp})]$ as functions of electric field (ξ) (Canali et al., 1971).
¶ $m_0 = 9.1 \times 10^{-31}$ Kg is the rest mass of an electron.
¶¶ $\varepsilon_s = \varepsilon_r\varepsilon_0$ is the permittivity of the semiconductor material; where $\varepsilon_0 = 8.85 \times 10^{-12}$ F m^{-1} is the permittivity of vacuum.

Source: Grant (1973), Canali et al. (1971), IOFFE (2019) and Zeghbroeck (2011)

Figure 2 Flowchart representing the workflow of the simulation study

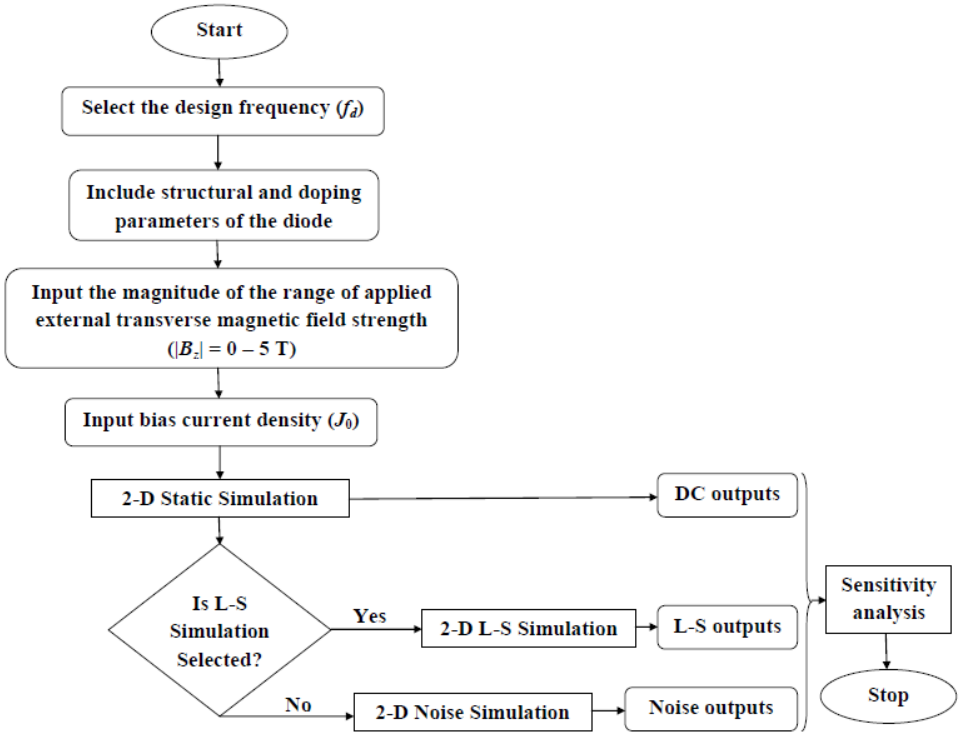

5 Results and discussion

The DC, L-S and noise characteristics of 94, 140, 220, 300 and 500 GHz DDR Si IMPATT diodes have been studied under transverse magnetic field. The simulation results have been presented and interpreted in best way in this section. The arrangement of modulation of IMPATT oscillator properties by applying external magnetic field as a whole is regarded as MAGTATT device (Banerjee et al., 2016a, 2018, 2016b).

5.1 Static properties

The DC parameters like breakdown voltage (V_B), avalanche zone voltage drop (V_A) and avalanche zone width (x_A) of the MAGTATT diodes operating at aforementioned mm-wave and THz frequencies have been obtained as the output of the 2D static simulation program. The simulations have been carried out for $|B_z| = 0$, 1, 2, 3, 4 and 5 T. The variations of V_B, V_A, $[(x_A/W) \times 100$; where $W = W_n + W_p$ is the depletion layer width] with operating frequency have been shown in Figure 3. It is observed from Figure 3 that V_B and V_A decrease with the increase of operating frequency. It is noteworthy to observe from that figure that x_A of the diodes increases rapidly with the increase of operating frequency.

The variations of the sensitivities of V_B, V_A and x_A with respect to the magnitude of the applied external transverse magnetic field have been shown in Figures 3(a)–3(c). All the sensitivities are found to be positive, i.e., V_B, V_A and x_A are increased due to the increase in strength of the applied transverse magnetic field. The above-mentioned sensitivities are found to be increasing with the increase of the magnetic field strength; the primary cause of these increments of magnetic field sensitivities of DC parameters have already been explained by the authors in their earlier report (Banerjee et al., 2016a).

Figure 3 Variations of breakdown voltage, avalanche zone voltage drop, percentage of avalanche zone width with respect to the depletion width with operating frequency under zero magnetic field

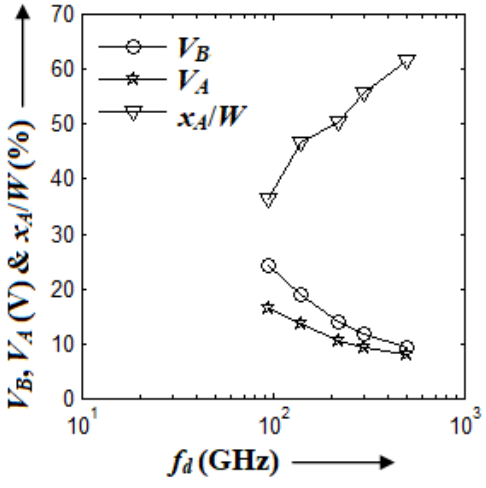

Figure 4 Variations of sensitivities of, (a) breakdown voltage (b) avalanche zone voltage drop (c) avalanche zone width with respect to the magnitude of the applied external transverse magnetic field

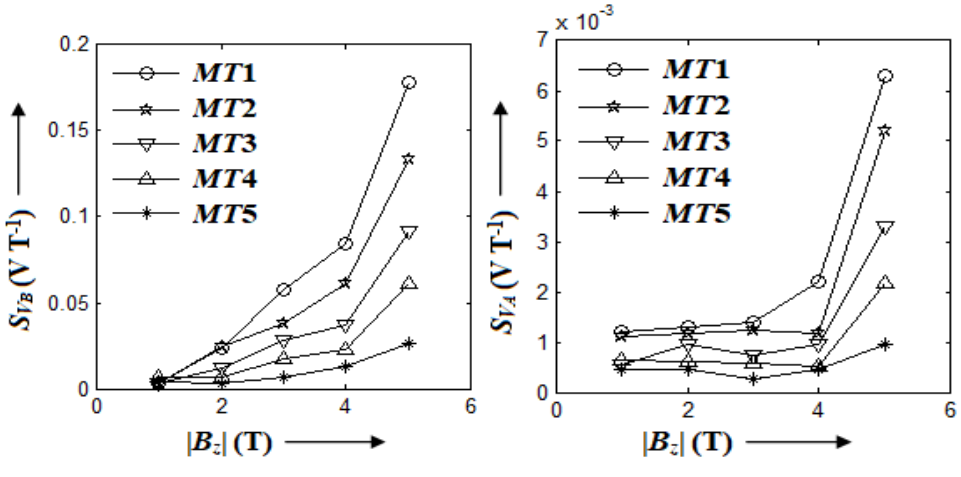

Figure 4 Variations of sensitivities of, (a) breakdown voltage (b) avalanche zone voltage drop (c) avalanche zone width with respect to the magnitude of the applied external transverse magnetic field (continued)

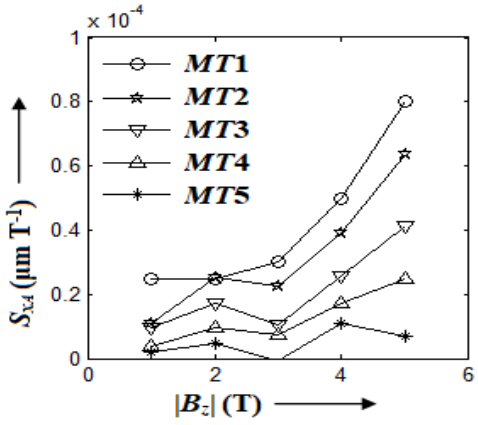

(c)

However, one noteworthy thing which can be observed from the current study is that the magnetic field sensitivities of DC parameters are significantly decreasing with the increase of the operating frequency. These decrements of magnetic field sensitivities with the operating frequency of the diodes can be explained as follows. The depletion width of MAGTATT diodes decrease rapidly with the increase of the operating frequency which can be observed from Figure 3. Therefore, in the higher frequency diodes, due to the narrower active layer thickness, the total amount of Hall deflection in mobile electrons and holes just before reaching the respective electrodes becomes smaller. Thus, the increase of the effective depletion region width (Banerjee et al., 2016a) due to the application of a particular value of magnetic field strength along the transverse direction of a higher frequency diode is significantly less as compared to that in a lower frequency diode. Consequently, the increments of V_B, V_A and x_A with the increase of $|B_z|$ are found to be smaller in higher frequency MAGTATT diodes as compared to their smaller frequency counterparts.

5.2 L-S properties

The important L-S parameters like optimum frequency (f_p) and RF power output (P_{RF}) of the MAGTATT diodes operating at aforementioned mm-wave and THz frequencies have been obtained as the output of the 2D L-S simulation program for $|B_z|$ = 0, 1, 2, 3, 4 and 5 T. The variations of P_{RF}, and f_p with operating frequency have been shown in Figure 5. It is observed that the power output decreases rapidly with the increase of operating frequency.

The variations of the sensitivities of P_{RF}, and f_p with respect to the magnitude of the applied external transverse magnetic field have been shown in Figures 6(a) and 6(b). It is observed that the magnetic field sensitivity of RF power output is positive, while the same of optimum frequency is negative for all the diodes under consideration. Therefore, RF power output and optimum frequency of a MAGTATT diode increases and decreases respectively with the increase of applied external transverse magnetic field. The primary

reasons of the said changes in P_{RF}, and f_p due to the change in $|B_z|$ have already been mentioned in the earlier paper (Banerjee et al., 2016a). The most important observation from Figures 3(b) and 9(c) that magnetic field sensitivities of P_{RF}, and f_p are very small in higher frequency diodes. The magnetic field sensitivity of PRF is found to be varying from 0.390 to 10.260 mW T^{-1} in 94 GHz diode, whereas range of the same is only 0.0492–1.2640 mW T^{-1} in 0.5 THz diode due to the change in the strength in applied transverse magnetic field from 0 to 5 T. Similarly, the ranges of the magnetic field sensitivity of 94 GHz and 0.50 THz diodes are found to be from –1.1218 to –6.9805 GHz T^{-1} and from –0.188 to –1.403 GHz T^{-1} respectively due to the change in $|B_z|$ within the range of 0–5 T.

Figure 5 Variations of RF power output, optimum frequency with design frequency under zero magnetic field

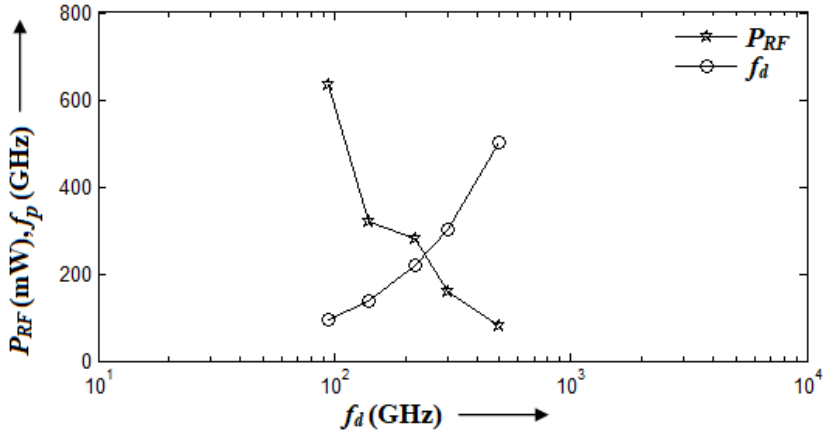

Figure 6 Variations of the sensitivities of, (a) RF power output (b) optimum frequency with respect to the magnitude of the applied external transverse magnetic field

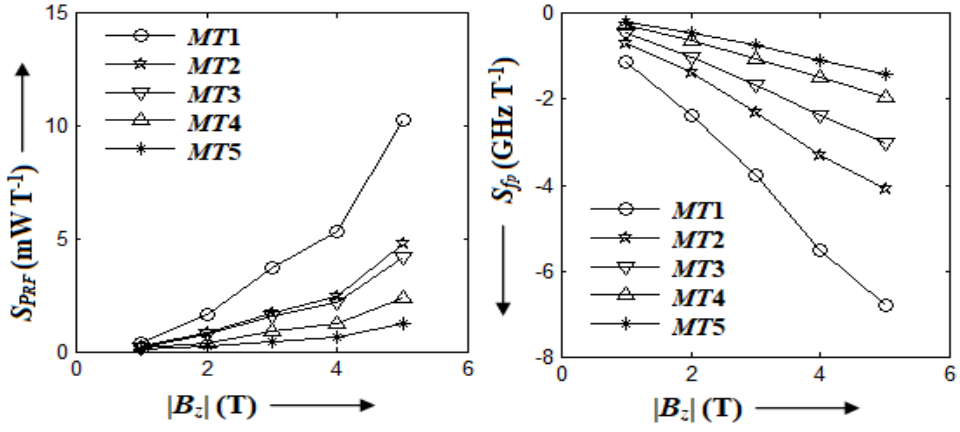

(a) (b)

5.3 Noise properties

Variation of noise measure (MN) with design frequency obtained from 2D noise simulation is shown in Figure 7. Obviously the noise measure decreases rapidly with the increase of operating frequency. It is observed from Figure 7 that the noise measure varies from 34.61 to 2.69 dB with the increase in the operating frequency from 94 GHz to 0.50 THz.

Figure 7 Variations of noise measure with design frequency under zero magnetic field

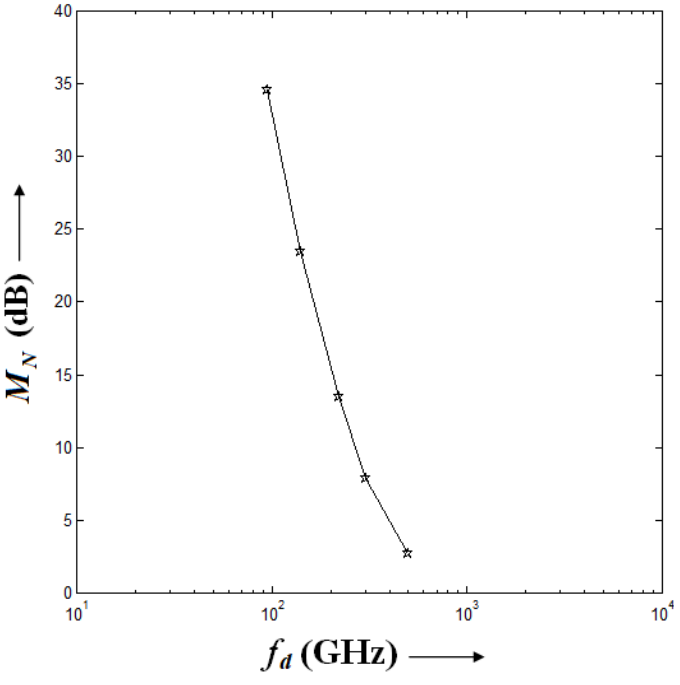

The depletion layer width of diodes is bound to be decreased significantly with the increase of the operating frequency of the diode following the transit time formula of Sze and Ryder (1971) given by $W_{n,p} = 0.37\ v_{sn,sp}/f_d$; where v_{sn} and v_{sp} are the saturation drift velocities of electrons and holes respectively and f_d is the design frequency. The optimised values of depletion layer widths (W_n and W_p) subject to obtain maximum DC to RF conversion efficiency at the concerned design frequency have been determined via a systematic optimisation technique discussed elsewhere (Acharyya et al., 2013b). Naturally the avalanche zone width also decreases with the increase of the operating frequency. Narrower avalanche zone in higher frequency diodes constitute less amount of random impact ionising collisions of charge particles within it; therefore, less random fluctuation in diode current. Thus, the decrease of noise measure with operating frequency shown in Figure 7 is obvious.

The magnetic field sensitivity of noise measure with the magnitude of the applied external transverse magnetic field obtained from 2D noise simulation is shown in

Figure 8. It is noteworthy to observe from Figure 8 that the range of magnetic field sensitivity of noise measure of 94 GHz, 140 GHz, 220 GHz, 0.30 THz and 0.50 THz diodes are observed to be 0.4000–2.1000, 0.2715–1.4253, 0.1560–0.8191, 0.0907–0.4763 and 0.0311–0.1632 dB T^{-1} respectively due to the variation of applied external transverse magnetic field strength from 0 to 5 T. Thus, very negligible change in noise measure is observed in the diodes operating in THz regime.

Figure 8 Variations of sensitivity of noise measure with respect to the magnitude of the applied external transverse magnetic field

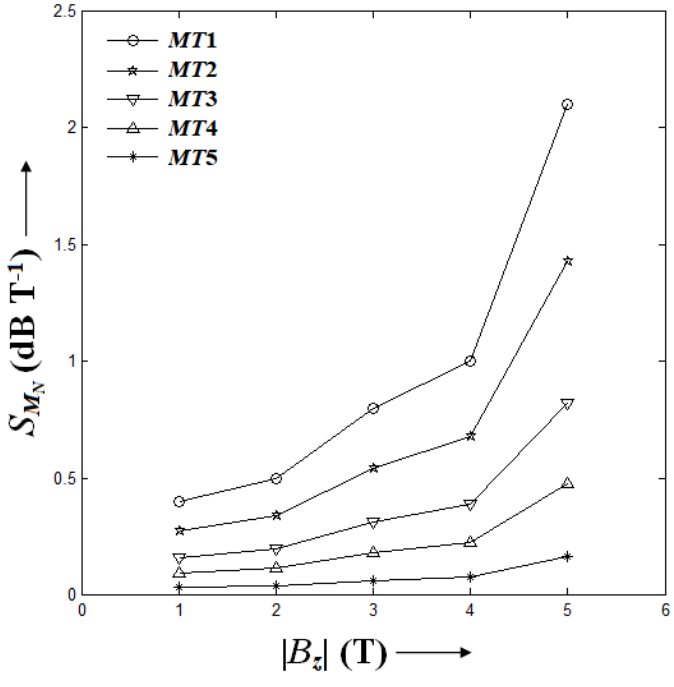

6 Conclusions

In this paper, the sensitivities of various static, L-S and noise characteristics of MAGTATT sources operating at 94, 140, 220 GHz and 0.30, 0.50 THz have been studied by using comprehensive 2D simulation models developed by the authors for evaluating static, large-signal and noise characteristics of MATATT diodes. The simulation results show that the above-mentioned magnetic field sensitivities of the device properties are significantly reduced with the increase of the operating frequency. One very important findings of this study is that the magnetic field sensitivities of noise measure of the diodes operating at THz frequencies are negligible; thus the MAGTATT operation is possible in THz regime without affecting the noise performance of the source.

Acknowledgements

Dr. Arindam Biswas wishes to thank Science and Engineering Research Board (SERB), India, for providing financial support for carrying out this research work through Early Career Research (ECR) Award scheme having the grant file number: ECR/2017/000024/ES. All the authors wish to thank Cooch Behar Government Engineering College, WB, India, for providing excellent research facilities for carrying out the present work.

References

Acharyya, A. and Banerjee, J.P. (2014) 'Prospects of IMPATT devices based on wide bandgap semiconductors as potential terahertz sources', *Applied Nanoscience*, Vol. 4, No. 1, pp.1–14.

Acharyya, A., Banerjee, S. and Banerjee, J.P. (2013a) 'Effect of junction temperature on the large-signal properties of a 94 GHz silicon based double-drift region impact avalanche transit time device', *Journal of Semiconductors*, Vol. 34, No. 2, pp.024001–024012.

Acharyya, A., Chakraborty, J., Das, K., Datta, S., De, P., Banerjee, S. and Banerjee, J.P. (2013b) 'Large-signal characterization of DDR silicon IMPATTs operating up to 0.5 THz', *International Journal of Microwave and Wireless Technologies*, Vol. 5, No. 5, pp.567–578.

Acharyya, A., Banerjee, S. and Banerjee, J.P. (2014a) 'Optical control of large-signal properties of millimeter-wave and sub-millimeter-wave DDR Si IMPATTs', *Journal Computational Electronics*, Vol. 13, No. 2, pp.408–424.

Acharyya, A., Goswami, J., Banerjee, S. and Banerjee, J.P. (2014b) 'Estimation of most favorable optical window position subject to achieve finest optical control of lateral DDR IMPATT diode designed to operate at W-band', *Radioengineering*, Vol. 23, No. 2, pp.739–753.

Acharyya, A., Banerjee, S. and Banerjee, J.P. (2014c) 'Effect of photo-irradiation on the noise properties of double-drift silicon MITATT device', *International Journal of Electronics*, Vol. 101, No. 9, pp.1270–1286.

Acharyya, A., Goswami, J., Banerjee, S. and Banerjee, J.P. (2015) 'Quantum corrected drift-diffusion model for terahertz IMPATTs based on different semiconductors', *Journal of Computational Electronics*, Vol. 14, No. 9, pp.309–320.

Baltes, H.P., Andor, L., Nathan, A. and Schmidt-Weinmar, H.G. (1984) 'Two-dimensional numerical analysis of a silicon magnetic field sensor', *IEEE Transactions on Electron Devices*, Vol. 31, No. 7, pp.996–999.

Banerjee, P., Acharyya, A., Biswas, A. and Bhattacharjee, A.K. (2016a) 'Effect of magnetic field on the RF performance of millimeter-wave IMPATT source', *Journal of Computational Electronics*, Vol. 15, No. 1, pp.210–221.

Banerjee, P., Hao, Q., Biswas, A., Bhattacharjee, A.K. and Acharyya, A. (2016b) 'Avalanche noise in magnetic field tunable avalanche transit time device', in *Proceedings of IEEE International Conference on Computer, Electrical and Communication Engineering (ICCECE)*, Kolkata, West Bengal, India, 16 and 17 December, pp.1–4, DOI: 10.1109/ICCECE.2016.8009570.

Banerjee, P., Acharyya, A., Biswas, A., Bhattacharjee, A.K. and Inokawa, H. (2018) 'Noise performance of magnetic field tunable avalanche transit time source', *International Journal of Electronics and Communication Engineering*, Vol. 12, No. 10, pp.718–728.

Biswas, A., Sinha, S., Acharyya, A., Banerjee, A., Pal, S., Satoh, H. and Inokawa, H. (2018) '1.0 THz GaN IMPATT source: effect of parasitic series resistance', *Journal of Infrared, Millimeter and Terahertz Waves*, DOI: 10.1007/s10762-018-0509-z.

Canali, C., Ottaviani, G. and Quaranta, A.A. (1971) 'Drift velocity of electrons and holes and associated anisotropic effects in silicon', *Journal of Physics and Chemistry of Solids*, Vol. 32, No. 8, pp.1707–1720.

Crowe, T.W., Hesler, J.L., Retzloff, S.A., Pouzou, C. and Schoenthal, G.S. (2011a) 'Solid state LO sources for greater than 2 THz', *2011 ISSTT Digest, 22nd Symposium on Space Terahertz Technology*, Tucson Arizona, USA, pp.1–4.

Crowe, T.W., Hesler, J.L., Retzloff, S.A., Pouzou, C. and Hester, J.L. (2011b) 'Multiplier based sources for frequencies above 2 THz', *36th International Conference on Infrared, Millimeter and Terahertz Sources (IRMMW-THz)*, pp.1–4.

Deal, W., Mei, X., Radisic, V., Leong, K., Sarkozy, S., Gorospe, B., Lee, J., Liu, P., Yoshida, W., Zhou, J., Lange, M., Uyeda, J. and Lai, R. (2010) 'Demonstration of a 0.48 THz amplifier module using InP HEMT transistors', *IEEE Microw. Wireless Compon. Lett*., Vol. 20, No. 5, pp.289–291.

Debus, C. and Bolivar, P.H. (2007) 'Frequency selective surfaces for high sensitivity terahertz sensing', *Appl. Phys. Lett*., Vol. 91, No. 18, p.184102.

Fitzgerald, A.J., Cole, B.E. and Taday, P.F. (2005) 'Nondestructive analysis of tablet coating thicknesses using terahertz pulsed imaging', *J. Pharm. Sci*., Vol. 94, No. 1, pp.177–183.

Forrest, J.R. and Seeds, A.J. (1978) 'Optical injection locking of impatt oscillators', *Electronics Letters*, Vol. 14, pp.626–627.

Gibbons, G. (1973) *Avalanche-diode Microwave Oscillators*, Oxford University Press, Oxford.

Gilden, M. and Hines, M.E. (1966) 'Electronic tuning effects in read microwave avalanche diode', *IEEE Trans. on Electron Devices*, Vol. 13, No. 1, pp.169–175.

Glance, B. (1973) 'A magnetically tunable microstrip IMPATT oscillator', *IEEE Transaction of Microwave Theory and Techniques*, Vol. 21, No. 6, pp.425–426.

Grant, W.N. (1973) 'Electron and hole ionization rates in epitaxial silicon at high electric fields', *Solid State Electronics*, Vol. 16, No. 1, pp.1189–1203.

Grischkowsky, D., Keiding, S., Exter, M. and Fattinger, C. (1990) 'Far-infrared time-domain spectroscopy with terahertz beams of dielectrics and semiconductors', *J. Opt. Soc. Am. B*., Vol. 7, No. 10, pp.2006–2015.

Hacker, J., Seo, M., Young, A., Griffith, Z., Urteaga, M., Reed, T. and Rodwell, M. (2010) 'THz MMICs based on InP HBT technology', in *IEEE MTT-S Int. Microw. Symp. Dig*., pp.1126–1129.

Hartnagel, H.L., Srivastava, G.P., Mathur, P.C. and Sharma, V. (1975) 'Effect of transverse magnetic field on the power output and frequency of IMPATT oscillators', *Physica Status Solidi*, Vol. 3, No. a, pp.1K147–1K149.

Heyminck, S., Güsten, R., Graf, U., Stutzki, J., Hartogh, P., Hübers, H.W., Ricken, O. and Klein, B. (2009) 'GREAT: ready for early science aboard SOFIA', *Proc. 20th Intl. Symp. Space THz Techn*., Charlottesville, VA, pp.315–317.

IOFFE (2019) *Electronic Archive: New Semiconductor Materials, Characteristics and Properties* [online] http://www.ioffe.ru/SVA/NSM/Semicond/index.html (accessed January 2019).

Jördens, C. and Koch, M. (2008) 'Detection of foreign bodies in chocolate with pulsed terahertz spectroscopy', *Opt. Eng*., Vol. 47, No. 3, p.37003.

Kitagawa, S., Mizuno, M., Saito, S., Ogino, K., Suzuki, S. and Asada, M. (2017) 'Frequency-tunable resonant-tunneling-diode terahertz oscillators applied to absorbance measurement', *Japanese Journal of Applied Physics*, Vol. 56, No. 5, p.58002-1.

Lai, R., Mei, X., Deal, W., Yoshida, W., Kim, Y., Liu, P., Lee, J., Uyeda, J., Radisic, V., Lange, M., Gaier, T., Samoska, L. and Fung, A. (2007) 'Sub 50 nm InP HEMT device with f_{max} greater than 1 THz', in *Proc. IEEE Int. Electron Devices Meeting 2007*, pp.609–612.

Lobisser, E., Griffith, Z., Jain, V., Thibeault, B., Rodwell, M., Loubychev, D., Snyder, A., Wu, Y., Fastenau, J. and Liu, A. (2009) '200-nm InGaAs/InP type-I DHBT employing a dual-sidewall emitter process demonstrating $f_{max} >> 800$ GHz and $f_T = 360$ GHz', in *Proc. IEEE Int. Conf. Indium Phosphide Related Materials*, pp.16–19.

Maestrini, A., Mehdi, I., Siles, J.V., Ward, J., Lin, R., Thomas, B., Lee, C., Gill, J., Chattopadhyay, G., Schlecht, E., Pearson, J. and Siegel, P. (2012) 'First demonstration of a tunable electronic source in the 2.5 to 2.7 THz range', *IEEE Trans. Terahertz Science Techn*., Vol. 3, No. 1, p.177.

Martyniuk, P., Antoszewski, J., Martyniuk, M., Faraone, L. and Rogalski, A. (2014) 'New concepts in infrared photodetector designs', *Appl. Phys. Rev.*, Vol. 1, No. 1, pp.41102-1-35.

Pfleiderer, H. (1972) 'Magnetodiode model', *Solid-State Electronics*, Vol. 15, No. 3, pp.335–353.

Pucel, R.A. and Masse, D.J. (1972) 'Microstrip propagation on magnetic substrates – part I: design theory', *IEEE Trans. Microwave Theory Tech*., Vol. 20, No. 5, pp.304–308.

Schweighart, A., Vyas, H.P., Borrego, J.M. and Gutmann, R.J. (1978) 'Avalanche diode structure suitable for microwave-optical interaction', *Solid-Sate Electron.*, Vol. 21, No. 9, pp.1119–1121.

Seeds, A.J. and Augusto, A. (1990) 'Optical control of microwave semiconductor devices', *IEEE Trans. on Microwave Theory and Techniques*, Vol. 38, No. 5, pp.577–585.

Seo, M., Urteaga, M., Hacker, J., Young, A., Griffith, Z., Jain, V., Pierson, R., Rowell, P., Skalare, A., Peralta, A., Lin, R., Pukala, D. and Rodwell, M. (2011) 'InP HBT IC technology for terahertz frequencies: fundamental oscillators up to 0.57 THz', *IEEE Journal of Solid-State Circuits*, Vol. 46, No. 10, pp.2203–2214.

Seo, M., Urteaga, M., Young, A., Jain, V., Griffith, Z., Hacker, J., Rowell, P., Pierson, R. and Rodwell, M. (2010) '300 GHz fixed-frequency and voltage-controlled fundamental oscillators in an InP HBT process', in *IEEE MTT-S Int. Microw. Symp. Dig*., pp.272–275.

Siegel, P.H. (2004) 'Terahertz technology in biology and medicine', *IEEE Trans. Microw. Theory Tech*., Vol. 52, No. 10, pp.2438–2447.

Siegel, P.H. (2007) 'THz instruments for space', *IEEE Transactions on Antenna and Propagation*, Vol. 55, No. 11, pp.2957–2965.

Stoik, C.D., Bohn, M.J. and Blackshire, J.L. (2008) 'Nondestructive evaluation of aircraft composites using transmissive terahertz time domain spectroscopy', *Opt. Express*., Vol. 16, No. 21, pp.17039–17051.

Sze, S.M. and Ryder, R.M. (1971) 'Microwave avalanche diodes', *Proc. of IEEE, Special Issue on Microwave Semiconductor Devices*, Vol. 59, pp.1140–1154.

Tonouchi, M. (2007) 'Cutting-edge terahertz technology', *Nature Photonics*, Vol. 1, No. 2, pp.97–105.

Urteaga, M., Seo, M., Hacker, J., Griffith, Z., Young, A., Pierson, R., Rowell, P., Skalare, A. and Rodwell, M. (2010) 'InP HBT integrated circuit technology for terahertz frequencies', in *Proc. IEEE Compound Semicond. Integr. Circuit Symp*., pp.1–4.

Vyas, H.P., Gutmann, R.J. and Borrego, J.M. (1979) 'Effect of hole versus electron photocurrent on microwave-optical interactions in impatt oscillators', *IEEE Transactions on Electron Devices*, Vol. 26, No. 3, pp.232–234.

Ward, J., Schlecht, E., Chattopadhyay, G., Maestrini, A., Gill, J., Maiwald, F., Javadi, H. and Mehdi, I. (2004) 'Terahertz technology in biology and medicine', *IEEE MTT-S Digest*., pp.1587–1590.

Williams, B.S. (2007) 'Terahertz quantum-cascade lasers', *Nature Photonics*, Vol. 1, pp.617–626.

Yasui, T., Yasuda, T., Sawanaka, K. and Araki, T. (2005) 'Terahertz paintmeter for noncontact monitoring of thickness and drying progress in paint film', *Appl. Opt*., Vol. 44, No. 1, pp.6849–6856.

Zeghbroeck, B.V. (2011) *Principles of Semiconductor Devices*, Colorado Press, USA.